Dynamics of downwelling in an eddying marginal sea
Contrasting the eulerian and the isopycnal perspective

Brüggemann, Nils; Katsman, Caroline A.

Important note
To cite this publication, please use the final published version (if applicable).
Please check the document version above.

Dynamics of Downwelling in an Eddying Marginal Sea: Contrasting the Eulerian and the Isopycnal Perspective

NILS BRÜGGEMANN[a] AND CAROLINE A. KATSMAN

Environmental Fluid Mechanics, Hydraulic Engineering Department, Faculty of Civil Engineering and Geosciences, Delft University of Technology, Delft, Netherlands

ABSTRACT

In this study, we explore the downward branch of the Atlantic meridional overturning circulation (AMOC) from a perspective in depth space (Eulerian downwelling) as well as from a perspective in density space (diapycnal downwelling). Using an idealized model, we focus on the role of eddying marginal seas, where dense water is formed by deep convection due to an intense surface heat loss. We assess where diapycnal mass fluxes take place, investigate the pathways of dense water masses, and elucidate the role of eddies. We find that there are fundamental differences between the Eulerian and diapycnal downwelling: the strong Eulerian near-boundary downwelling is not associated with substantial diapycnal downwelling; the latter takes place in the interior and elsewhere in the boundary current. We show that the diapycnal downwelling appears to be more appropriate to describe the pathways of water masses. In our model, dense water masses are exported along two routes: those formed in the upper part of the boundary current are exported directly; those formed in the interior move toward the boundary along isopycnals due to eddy stirring and are then exported. This study thus reveals a complex three-dimensional view of the overturning in a marginal sea, with possible implications for our understanding of the AMOC.

1. Introduction

In the marginal seas of the North Atlantic, intense net downward motions connect the upper northward branch of the Atlantic meridional overturning circulation (AMOC) to its lower southward branch. While at a first glance, it may seem appealing to associate the sinking of dense water masses in the North Atlantic with deep convection in these marginal seas, Send and Marshall (1995) showed based on theoretical arguments and by means of idealized numerical model studies that the net vertical motion over areas subject to deep convection is relatively small. That is, the downward flow required to connect the upper and lower branches of the AMOC has to occur outside the deep convection areas

(Marotzke and Scott 1999; Spall and Pickart 2001). Indeed, idealized model studies (e.g., Spall 2003, 2004, 2010; Georgiou et al. 2019) and realistic model studies (Katsman et al. 2018; Waldman et al. 2018; Sayol et al. 2019) have shown that intense downwelling occurs within the buoyant boundary currents of the subpolar gyre rather than in the ocean interior. Regions with strong eddy activity are regions where this near-boundary sinking peaks (Spall 2003, 2004, 2010; Georgiou et al. 2019; Sayol et al. 2019).

The basic mechanism behind the overturning in a marginal sea subject to intense heat loss lies in the densification of the buoyant boundary current, due to strong surface heat losses and/or lateral eddy heat fluxes (Spall and Pickart 2001; Spall 2003, 2004; Straneo 2006). As a consequence of this densification of the boundary current, the horizontal density gradient between the boundary current and the interior reduces in the downstream direction, and therewith the thermal wind shear decreases. This causes a deceleration of the upper part of the boundary current and an acceleration of its lower part; a process usually referred to as barotropization of the boundary current (Spall and Pickart 2001; Spall 2004; Walin et al. 2004; Straneo 2006).

---

[a] Current affiliation: University of Hamburg, Hamburg, Germany.

Corresponding author: Nils Brüggemann, nils.brueggemann@uni-hamburg.de

This barotropization implies overturning somewhere in the basin reflecting the transfer of water from the upper part of the boundary current toward its lower part. If this downwelling were to occur within the stratified boundary current, as suggested by among others the two-layer model of Straneo (2006), it needs to cross isopycnals. However, the time-mean near-boundary sinking typically occurs well below the local mixed layer depth (Spall 2004; Katsman et al. 2018; Georgiou et al. 2019) where diapycnal processes are small and water masses are expected to follow isopycnals.

Indeed, Spall (2010) demonstrated that a strong shedding of mesoscale eddies at a topographic narrowing in the marginal sea is accompanied by an eddy bolus flow. Such an eddy bolus flow was already proposed by, for example, Jones and Marshall (1997) and Khatiwala and Visbeck (2000), who suggested that the restratifying eddy circulation might play an important role for the export of freshly formed Labrador Seawater. In Spall (2010), the eddy bolus flow counteracts the time mean downward flow through a depth level (Eulerian downwelling), and the residual flow—defined as the sum of Eulerian and bolus flow—is upward rather than downward, and indeed mostly along the isopycnals. Furthermore, Cessi and Wolfe (2013) used the thickness-weighted average formulation (Young 2012) to study the isopycnal circulation in eastern boundary currents with enhanced eddy activity. They showed that the vertical zonal mean and eddy components of the residual transport balance and that a net residual downward transport is absent along the eastern boundary current below the mixed layer despite strong Eulerian downwelling in depth space. Therefore, they concluded that the eastern boundary current is not the downwelling limb of a zonal or meridional overturning circulation.

Further doubt on the importance of the intense Eulerian downwelling along a topographic narrowing for the formation, overturning and the export of dense water masses is raised by the study by Brandt et al. (2007). Using an artificial subduction tracer and Lagrangian particles in an eddy-resolving model study of the North Atlantic, they found that nearly all the dense water that exits the Labrador Sea via the Labrador Current has been formed just upstream of this location, adjacent to the Labrador Current. In particular, this pathway does not pass through the area of intense eddy shedding and sinking along the west coast of Greenland (Spall 2010; Katsman et al. 2018; Georgiou et al. 2019). Rather, diapycnal fluxes along the west coast of Greenland diagnosed from an isopycnal model study in Xu et al. (2018) are indicative of local upwelling, as they are directed from dense to light water masses.

The question thus remains which path the dense water masses take from their formation region until they exit the marginal sea via the boundary current, and what role the prominent eddy field plays for exporting this water. In this study, we present an integrative view of the downwelling that connects recent studies about vertical mass fluxes in a marginal sea (Spall 2004, 2010; Katsman et al. 2018) with studies on diapycnal water mass transformation and the isopycnal circulation (Brandt et al. 2007; Cessi and Wolfe 2013; Xu et al. 2018). In particular, we contrast the Eulerian downwelling with the diapycnal and isopycnal circulation in an idealized model configuration of a marginal sea typical for the North Atlantic, similar to idealized models applied before to study the convective cycle, overturning, and heat transport in marginal seas (Spall 2004, 2010; Georgiou et al. 2019). We diagnose the flow in density space, identify where diapycnal mass transports occur, and chart which pathways dense water masses take upon exiting a marginal sea that is subject to deep convection and displays strong eddy activity. We elucidate how eddies provide a complex connection between the downwelling in depth space, the overturning, and the pathways of dense water. Furthermore, the results of this study can help interpreting observational estimates of the overturning as, for example, obtained from the Overturning in the Subpolar North Atlantic Program (OSNAP) array (Holliday et al. 2018; Lozier et al. 2019).

In the following, we first introduce the numerical model (section 2) and the diagnostics that we use (section 3). Next, we discuss the barotropization of the boundary current that is inherent to the overturning and export of water masses (section 4) before we use the isopycnal framework to discuss how this barotropization is achieved (section 5). The pathways of dense water masses that illustrate the circulation obtained from the isopycnal framework are investigated in section 6 by means of a passive tracer study. Finally, section 7 contains the summary and conclusion of our results.

2. Model configuration

The model configuration of the MITgcm (Marshall et al. 1997) used in this study mimics the circulation in the marginal seas of the North Atlantic and is very similar to that applied in Spall (2010). It is especially designed for situations where buoyant (typically warm) water is transported from a boundary current into a less buoyant (typically cold) interior by eddies. In this regard, it is typical for the Labrador Sea and the Lofoten basin but might as well reflect the situation at other locations. In the southernmost part, a warm stratified boundary current is forced by restoring temperature and
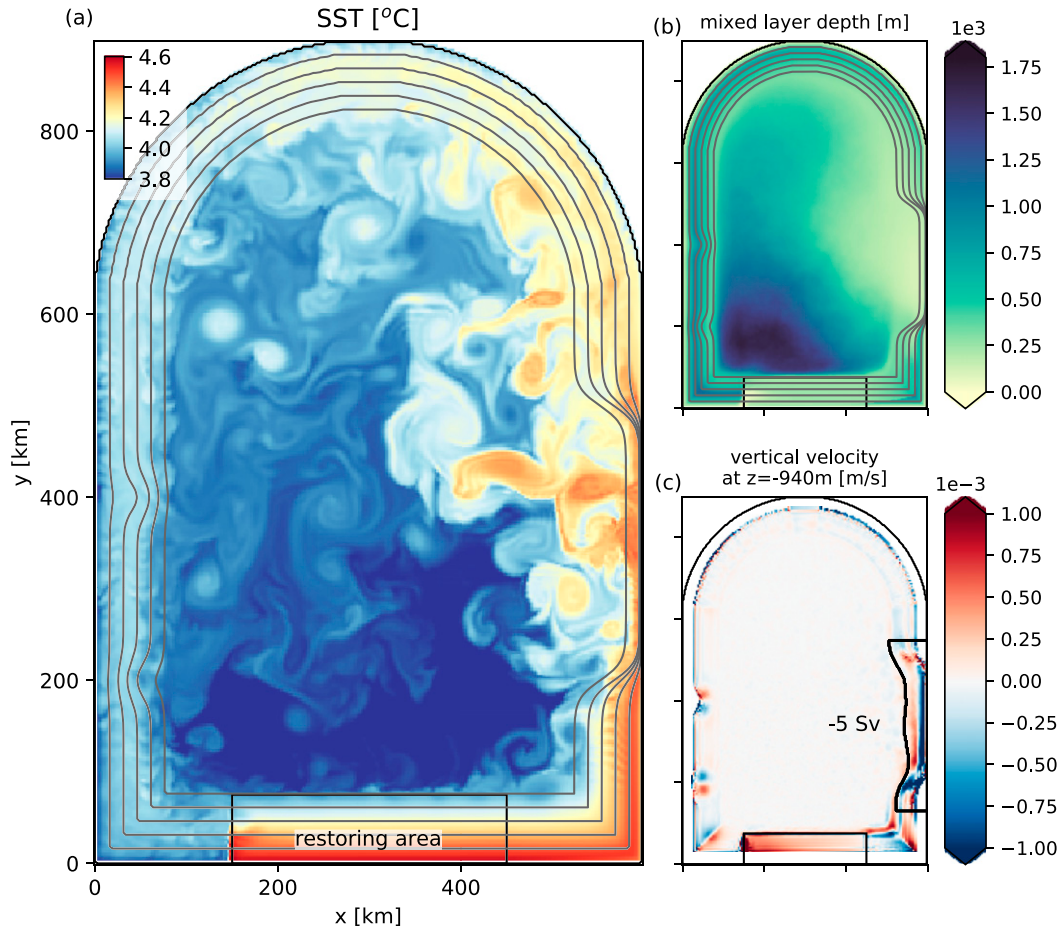
FIG. 1. Characteristics of the idealized model simulation: (a) snapshot of sea surface temperature after 10.5 years; (b) time average (years 10–20) of the mixed layer depth; (c) time average (years 10–20) of the vertical velocity at $z = 940$ m. Gray lines in (a) and (b) denote isobaths with intervals of 500 m; the black rectangle in the south denotes the restoring area. The thick black contour in (c) denotes the area for which the downwelling in depth space is derived. It is bounded in the west by the 24-Sv contour of the barotropic streamfunction (see section 4 for details).

velocity (Fig. 1a) such that the vertical stratification of the boundary current is $N^2 = 0.25 \times 10^{-6}\,\mathrm{s}^{-1}$ and the horizontal stratification is in thermal wind balance with a velocity profile that is linearly decreasing from zero at the bottom to $0.5\,\mathrm{m\,s}^{-1}$ at the surface. This boundary current follows the linearly sloping topography around the basin. At the eastern side of the basin, similar to the situation in the Labrador Sea or the Norwegian Sea, the topographic slope steepens, the boundary current becomes unstable and warm-core anticyclonic eddies are shed. A constant and uniform cooling of $50\,\mathrm{W\,m}^{-2}$ is applied, which leads to deep convection in the interior (Fig. 1b). Along the boundary, this heat loss is balanced by the alongshore advection of heat by the boundary current. In contrast, in the interior the surface heat loss is balanced by the lateral heat transfer by warm-core eddies shed from the boundary current. The warm, stratified water carried by the eddies

hampers deep convection, so that the deepest mixed layers are found in the southwest, where the influence of the eddies is smallest (Fig. 1b).

Further idealizations of the model are a linear equation of state with temperature as the only active tracer, and a β-plane approximation where the Coriolis parameter f is given by $f = f_0 + \beta y$ with $f_0 = 1 \times 10^{-4}\,\mathrm{s}^{-1}$ and $\beta = 1 \times 10^{-11}\,\mathrm{m}^{-1}\,\mathrm{s}^{-1}$. The horizontal resolution is 2.5 km and the vertical resolution ranges from 20 m at the surface up to 280 m at a maximum depth of 3000 m with 20 levels in total. Subgrid scale horizontal friction and diffusion are parameterized by a biharmonic operator with a constant viscosity of $A_4 = 6.25 \times 10^7\,\mathrm{m}^4\,\mathrm{s}^{-1}$ and a constant diffusivity of $k_4 = 6.25 \times 10^7\,\mathrm{m}^4\,\mathrm{s}^{-1}$. Vertical friction and diffusion are parameterized by a turbulent kinetic energy scheme (Gaspar et al. 1990) and in case of an unstable stratification, the vertical diffusivity is increased to $10\,\mathrm{m}^2\,\mathrm{s}^{-1}$. In addition to the vertical

friction, we apply quadratic bottom friction with a drag coefficient of 3×10^{-3}. After roughly 7 years, the mean temperature and kinetic energy within the basin are in a quasi-steady state; time-averaged diagnostics are performed for the years 10–20 of the simulation.

As expected, the time-averaged vertical velocity at 940-m depth (Fig. 1c) displays intense vertical motions along the topographic narrowing in the east, at two topographic obstacles in the west, in the southeastern and southwestern corners and within the restoring area. However, the downward motions along the topographic narrowing dominate the overall Eulerian sinking in the model [which amounts to 5 Sv ($1\,\mathrm{Sv} \equiv 10^{6}\,\mathrm{m^{3}\,s^{-1}}$) at this depth, see indicated region in Fig. 1c], where convection is shallow (Fig. 1b). Up- and downwelling at topographic features cancel each other. Finally, there is intense upwelling in the restoring area that closes the overturning loop in depth space.

Note that we do not consider effects of salinity and only use temperature variations to represent density variations. While the warm boundary currents of the North Atlantic are typically saline, the water masses at the shelf usually contain meltwater and have very low salinity. If these freshwater masses are advected from the shelf into the interior of the marginal seas by eddies, the water column is stabilized and convection can be limited (e.g., Dickson et al. 1988; Gelderloos et al. 2012). Since our main focus is to provide a qualitative picture of the circulation in a marginal sea characterized by deep convection and eddies that transfer stratified buoyant water masses from the boundary current toward the convection area, the effects of salinity are omitted in our setup. The model domain, properties of the boundary current, and the surface forcing are chosen such that a good representation of the eddy field and the interaction between eddies and deep convection is achieved while still allowing for a transparent analysis. Hence, this idealized model is judged fit for the purpose of this study despite the idealizations that are applied. It is anticipated that the outcomes will help diagnose these processes in more complex models (e.g., Xu et al. 2018) or observations (e.g., Holliday et al. 2018; Lozier et al. 2019) in a more quantitative way. Furthermore, using such an idealized model has the advantage that the processes under consideration can be studied in a relatively isolated way. Complications by complex bathymetry or by a spatially or temporally varying forcing can be omitted and the interpretation of complex phenomena is facilitated.

3. Diagnostics for the isopycnal framework

To assess where diapycnal water mass transformation occurs and where these water masses are transported,

we diagnose the isopycnal circulation and diapycnal flows (section 5). We define the vertically integrated horizontal flow above a certain density surface at depth $z(x, y, \rho)$ as

$$\overline{\mathbf{U}}_{\rho}(x, y, \rho) = \overline{\int_{z(x,y,\rho)}^{\eta(x,y)} \mathbf{u}_{h}\, dz}. \tag{1}$$

In Eq. (1), an overbar indicates a time average, ρ is density, $\mathbf{u}_{h} = (u, v)^{\mathrm{T}}$ the horizontal velocity vector, and $\eta(x, y)$ the sea surface elevation. Recall that we use a linear equation of state with temperature as the only active tracer so that isopycnal interfaces coincide with isothermal interfaces. Technically, $\mathbf{U}_{\rho}$ is calculated online in the model at each model time step using the LAYERS package (Abernathey et al. 2013) of the MITgcm (Adcroft et al. 1997), using steps of 0.05°C as the layer increment.

An equation for the time averaged layer thickness $\overline{h}_{\rho} = \overline{\int_{z(x,y,\rho)}^{\eta(x,y)} dz}$ can also be derived from the density budget and the continuity equation [see, e.g., Olbers et al. (2012, their Eq. B.6) but note that we integrated over density]:

$$\partial_{t_{\rho}} \overline{h}_{\rho} + \nabla_{\rho} \cdot \overline{\mathbf{U}}_{\rho} = \overline{Q}. \tag{2}$$

Here, $\partial_{t_{\rho}}$ is a derivative with respect to time at constant density, $\nabla_{\rho} \cdot$ is the horizontal divergence at constant density, and Q denotes a source term for $\overline{h}_{\rho}$ due to surface buoyancy fluxes and due to diapycnal mixing.

We define the layer interface velocity $\overline{w}_{\rho}$ as (see also Young 2012)

$$\overline{w}_{\rho} := \nabla_{\rho} \cdot \overline{\mathbf{U}}_{\rho} = \overline{Q} - \partial_{t_{\rho}} \overline{h}_{\rho}. \tag{3}$$

In a steady state where $\partial_{t_{\rho}} \overline{h} = 0$, $\overline{w}_{\rho}$ denotes a diapycnal velocity between the upper and the lower isopycnal layer (referred to as diapycnal downwelling when directed from the lighter into the denser isopycnal layer, and as diapycnal upwelling when directed oppositely; the downward flow associated with a vertical velocity at a specific depth level is referred to as downwelling in depth space or Eulerian downwelling).

To distinguish eddy and mean flow components of the isopycnal flow, we split the isopycnal transport into time mean and fluctuating parts following McDougall and McIntosh (2001):

$$\overline{\mathbf{U}}_{\rho}(x, y, \rho) = \underbrace{\int_{\overline{z}(x,y,\rho)}^{\overline{\eta}(x,y)} \overline{\mathbf{u}}_{h}\, dz}_{\overline{U}_{\rho,m}(x,y,\rho)} + \underbrace{\overline{\int_{z(x,y,\rho)}^{\overline{z}(x,y,\rho)} \mathbf{u}_{h}\, dz} + \overline{\int_{\overline{\eta}(x,y)}^{\eta(x,y)} \mathbf{u}_{h}\, dz}}_{\overline{U}_{\rho,e}(x,y,\rho)}. \tag{4}$$
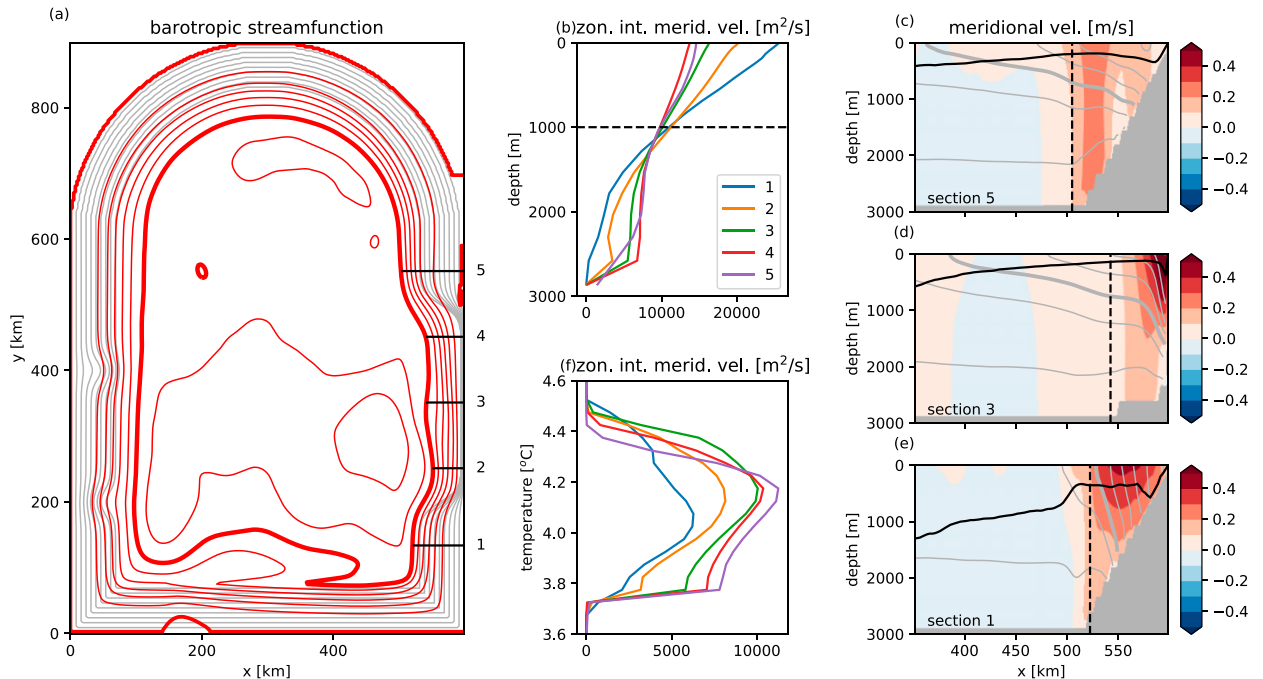
FIG. 2. (a) Ten-year averaged barotropic streamfunction (red contours; contour interval is 4 Sv). The 24-Sv contour line, which distinguishes the boundary current from the interior, is highlighted by the thick red line; gray lines indicate bathymetry. (b) Meridional velocities zonally integrated over the boundary current width (defined by the 24-Sv contour line) for different sections as indicated by the horizontal black lines in (a). (f) As in (b), but in temperature space. (c)–(e) Meridional velocities at sections 5, 3, and 1, respectively. Temperature is indicated by gray contours (contour interval is 0.1°C); the 4°C isotherm is highlighted by the thick gray line. The vertical dashed line denotes the location of the 24-Sv contour line and therewith the area over which the meridional velocities are integrated in (b); the black solid line denotes the mixed layer depth.

4. Barotropization of the boundary current

Spall (2004) and Straneo (2006) suggested that the amount of overturning that occurs in a marginal sea can be assessed based on the barotropization of the boundary current, as it reflects the transfer of waters from the upper part of the boundary current into its lower part (see also section 1). To investigate the changes in the vertical distribution of the boundary current transport in our idealized model simulation, we calculate the meridional transport across different sections along the eastern part of the domain (Fig. 2b). We define the boundary current as the area between the solid boundary and the 24-Sv streamline of the barotropic streamfunction (thick red line in Fig. 2a). With this definition, the total depth-integrated boundary current transport is constant along its path [as assumed in Spall (2004) and Straneo (2006)], even though its width changes [unlike in Spall (2004) and Straneo (2006), who assumed a constant width].

Just upstream of the narrowing, the flow is strongly sheared and the transport in its upper part is much larger than in its lower part (blue line in Fig. 2b). Following the boundary current further downstream, barotropization clearly takes place: along the narrowing, the transport above 940 m decreases and that below 940 m increases (yellow, green, and red lines). Note that downstream of the narrowing (violet line), the situation does not revert to the situation upstream of the narrowing (blue line): at its downstream end, there is substantially more transport in the lower part of the boundary current and less transport in the upper part than at its upstream end.

A more detailed picture of the changes in the vertical structure of the boundary current is obtained from three sections of the meridional velocity (Figs. 2c–e). These clearly show that the flow does not only become more barotropic but that also the transport within isopycnal layers changes: the transport above the 4°C isotherm (thick gray line) decreases while the transport below that isotherm increases. This becomes more obvious when we consider the meridional velocity in density space $\bar{v}_\rho$ averaged zonally over the boundary current width (Fig. 2f). Comparable to the barotropization in depth space (Fig. 2b), barotropization also takes place in

where we introduced the mean component $\overline{U}_{\rho,m}$ and the eddy component $\overline{U}_{\rho,e}$ (also called quasi-Stokes streamfunction) of the isopycnal velocity.

density space: downstream of the narrowing, the velocity in the upper layers has decreased while the velocity in the lower layers has increased. The vertical shear in density space gets smaller similar to the situation in depth space. Note that such a barotropization can be inferred from current measurements of the boundary currents of the Labrador Sea as well. While the northward West Greenland Current in the east of the Labrador Sea is strongly sheared, the southward Labrador Current in the west of the Labrador Sea displays less vertical shear (e.g., Pickart and Spall 2007; Hall et al. 2013).

5. Diapycnal fluxes and isopycnal circulation

Given the intense Eulerian downwelling signal within the boundary current along the topographic narrowing (Fig. 1c), it is appealing to conclude from the transport changes displayed in Fig. 2 that a strong diapycnal flux from the upper layers into the lower layers occurs within the boundary current. However, the boundary current is strongly stratified and the mixed layer along the eastern boundary is very shallow (Fig. 1b, black line in Figs. 2c–e). Therefore, it is questionable if a strong diapycnal flow actually occurs in this region.

a. Diapycnal fluxes

Before we analyze the diapycnal flow, we first consider the time-averaged depth $\overline{h}_\rho$ of three isotherms (Figs. 3a–c). As expected, the isotherm is found at the most shallow depth in the interior where deep convection occurs, and deepest in the warm boundary current. However, along its way around the basin perimeter, the boundary current cools and the isotherms rise. From Eq. (2), we deduce that intense diabatic transports can be expected where the isotherm outcrops in the mixed layer such that the diabatic forcing $\overline{Q}$ is large. A rough estimate of where this may occur is given by the black contours in Figs. 3a–c, which depict where the time-mean mixed layer depth equal the time-mean depth of this particular isotherm. From Fig. 3b for instance, it is evident that the 4.0°C isotherm is located below the mixed layer over large parts of the boundary current. It outcrops in the interior and within the southwestern part of the boundary current, suggesting that diapycnal mass transport is limited to these regions.

Indeed, the analysis of $\overline{w}_\rho$ (Figs. 3d–f) shows that diapycnal fluxes are low when the isopycnal is below the mixed layer. In particular within the boundary current, hardly any diapycnal fluxes can be found upstream of the location where isopycnals outcrop into the mixed layer (black contour line in Figs. 3d–f). However, when the boundary current becomes sufficiently cold such that it intersects with the mixed layer, diapycnal processes and therewith diapycnal velocities become important. This happens in the northwest for the lighter 4.1°C isotherm (Fig. 3d), in the southwest for the intermediate 4.0°C isotherm (Fig. 3e), and not at all for the 3.9°C isotherm (Fig. 3f). In addition, a less intense but widespread downward diapycnal flux can be seen over large parts of the basin interior, offshore of the narrowing and outside the boundary current (Figs. 3d–f). Over the entire domain, the downwelling needs to be compensated by upwelling. This mainly occurs within the restoring area where strong diapycnal fluxes are applied but also to a much lesser degree within the boundary current along the narrowing. Here, a weak diapycnal upwelling within the boundary current is seen (red shading in Figs. 3d and 3e). Diapycnal fluxes in our simulation might either be caused by the vertical diffusion of the TKE scheme or by the biharmonic diffusion which is enhanced in this area of sharp horizontal gradients. The latter is probably the main contributor for the upwelling along the narrowing and might be reduced if resolution is increased and the biharmonic diffusivities are reduced accordingly. These results are qualitatively in line with the water mass transformation obtained from the isopycnal model study by Xu et al. (2018), that is, the transformation of lighter water masses takes place continuously along the boundary current of the subpolar gyre (their Figs. 12d–f) while for denser water masses, it takes place offshore of the boundary current and in the interior of the Labrador Sea (their Figs. 12g,h).

b. Isopycnal circulation

To explore the isopycnal circulation, we show the isopycnal transport $\overline{\mathbf{U}}_\rho$ derived from Eq. (1) above and below the 4.1°C isotherm in Fig. 4. In the upper layer (Figs. 4a,c), the circulation is dominated by the strong boundary current. In the northwest of the domain, where the 4.1°C isotherm outcrops in the mixed layer (black line), the upper layer flow converges and a strong diapycnal flow from the upper into the lower layer can be observed (Fig. 3d). Notably, the upper layer flow also converges offshore of the narrowing, where part of the upper layer boundary current is deflected into the interior (Fig. 4c).

In the lower isopycnal layer (Figs. 4b,d), there is hardly any boundary current transport upstream of the topographic narrowing in the southeast of the domain. Along the narrowing, cold water from the interior is entrained into the boundary current (Fig. 4d). In the northwest, where surface fluxes cool the boundary current sufficiently so that the surface temperature reaches 4.1°C or less, there is a diapycnal transport from the warmer into the colder layer. Finally, the lower layer
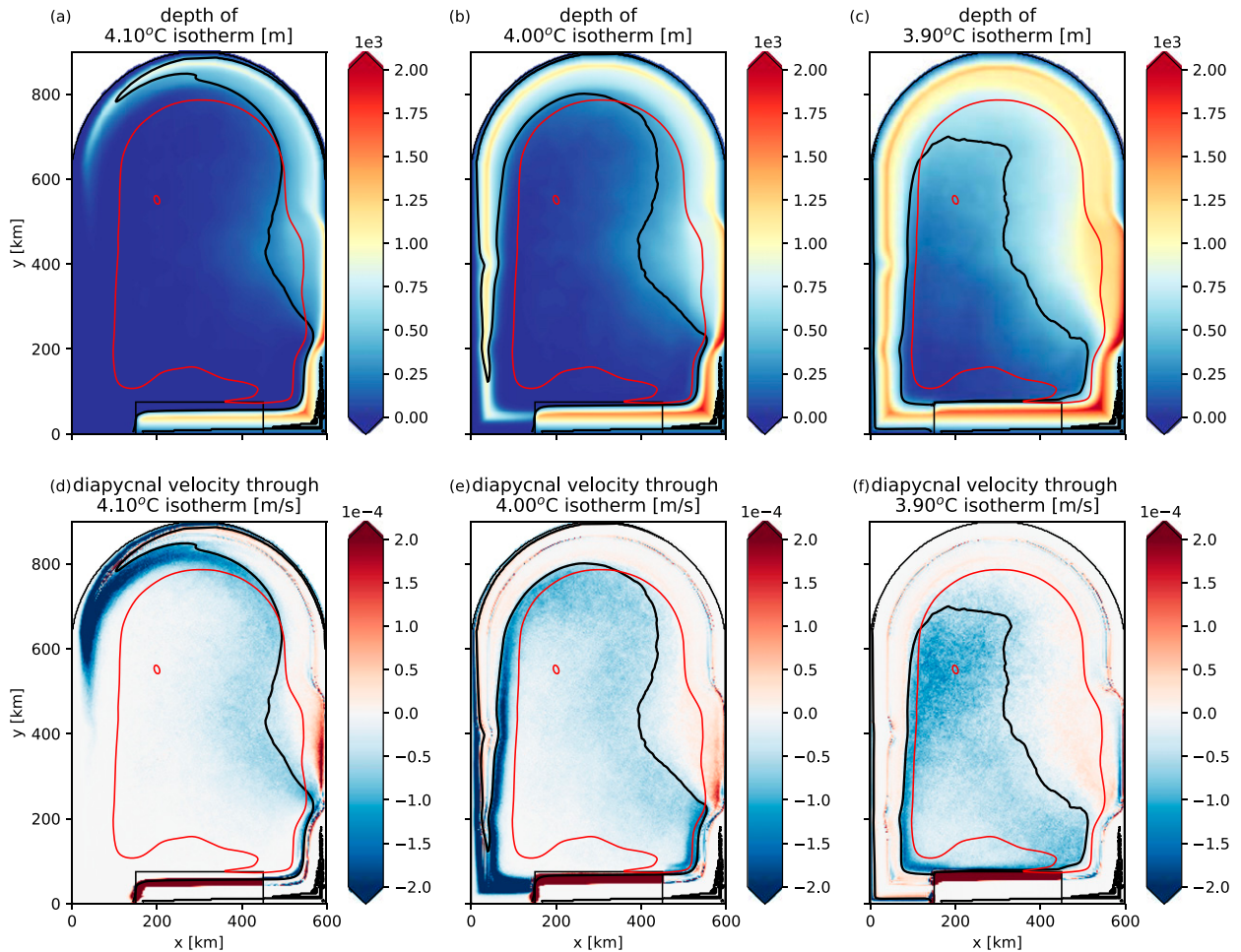
FIG. 3. (a)–(c) Time mean depth of three isotherms: (a) 4.1°, (b) 4.0°, and (c) 3.9°C. (d)–(f) Diapycnal velocities through the isotherms: (d) 4.1°, (e) 4.0°, and (f) 3.9°C. In accordance with Eq. (3), negative values indicate a diapycnal flow from the upper lighter layer into the lower heavier layer and vice versa. In all panels the restoring area is indicated by the black rectangle. The black contour indicates where the time mean depth of the corresponding isotherm intersects the time mean mixed layer depth; the red contour depicts the edge of the boundary current defined by the 24-Sv streamline of the barotropic flow (see Fig. 2).

water masses in the interior recirculate along complex pathways which mainly reflect the barotropic circulation before they eventually enter the boundary current again, that is, along the narrowing. The lower layer water masses in the boundary current mostly enter the restoring area, where they are forced to upwell diapycnally into the upper layer (e.g., Fig. 3d). We refer to these water masses as water masses that are exported out of the marginal sea since in a more realistic setup they would leave the marginal sea to be diapycnally transformed into lighter water masses somewhere else in the World Ocean, closing the global overturning loop.

c. Eddy–mean flow decomposition

The isopycnal exchange of water masses between the boundary current and the interior along the narrowing (Figs. 4c,d) strongly suggests that the eddy field plays a role. For a closer view on the role of the eddies, we split the isopycnal transport into its mean and eddy components following Eq. (4). Along the narrowing, we find intense up- and downwelling in both the mean and the eddy components of the flow (Figs. 5a,d), which nearly cancel each other; recall that their sum (Fig. 3d) displays relatively small diapycnal velocities. Such a pattern is typical for the eddy-induced overturning in the case of baroclinic instability of a front (e.g., Jones and Marshall 1997; Khatiwala and Visbeck 2000): the joined effect of the eddies is to lift water masses on the warmer side of the front and to push them down on the colder side in order to flatten the isopycnals (Fig. 5d). In a steady state, this eddy-induced overturning of the isopycnals needs to be counteracted by the mean flow and consequently, we find mean upwelling (downwelling) on the warmer (colder) side of the front associated with the boundary
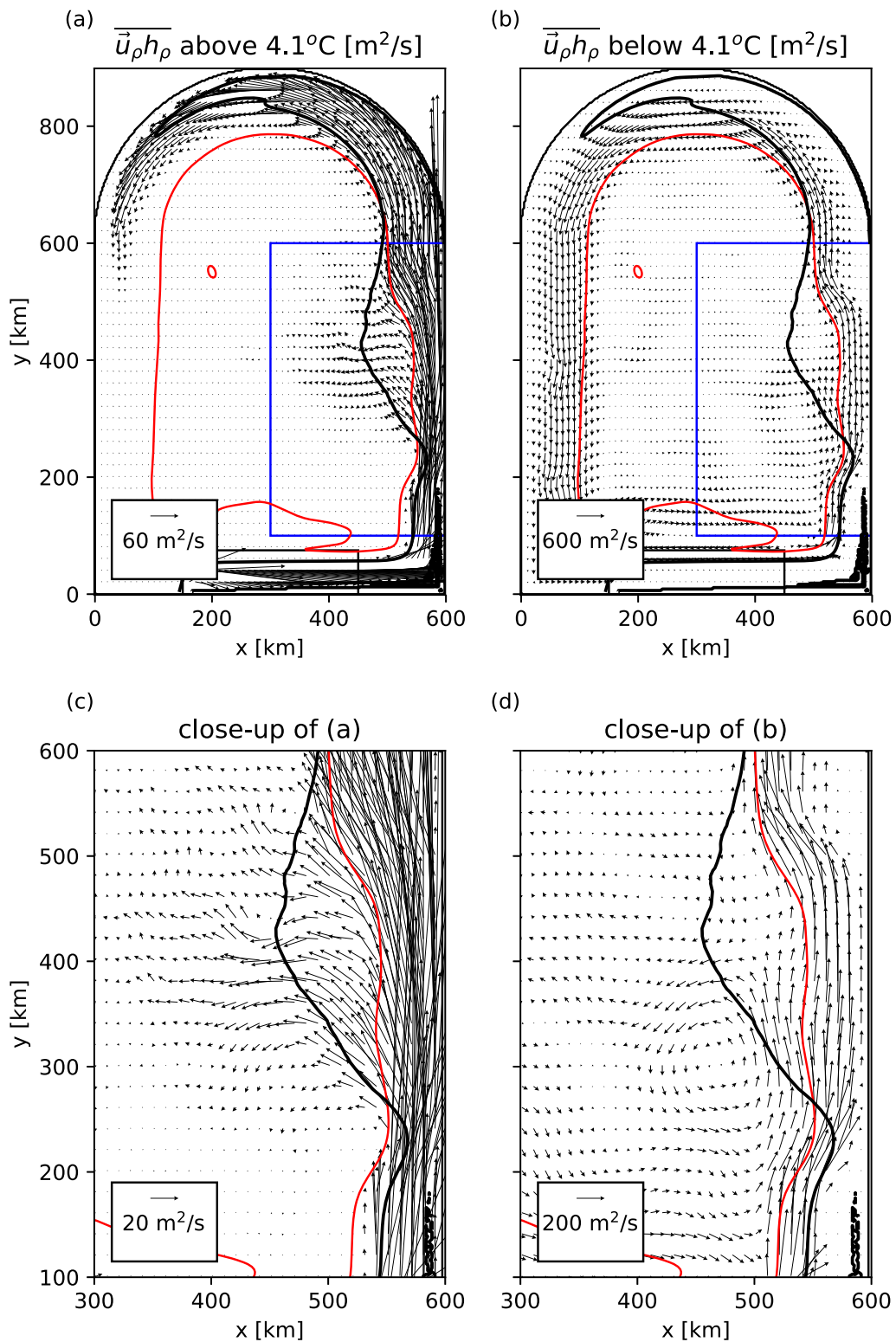
FIG. 4. Isopycnal flow (a),(c) below and (b),(d) above the 4.1°C isotherm for (top) the full domain and (bottom) close-ups along the topographic narrowing [indicated by the blue rectangles in (a) and (b)]. Note the different transport scales in all panels. As in Fig. 3, the black contour indicates where the time mean depth of the 4.1°C isotherm intersects the time mean mixed layer depth; the red contour depicts the edge of the boundary current defined by the 24-Sv streamline of the barotropic streamfunction.
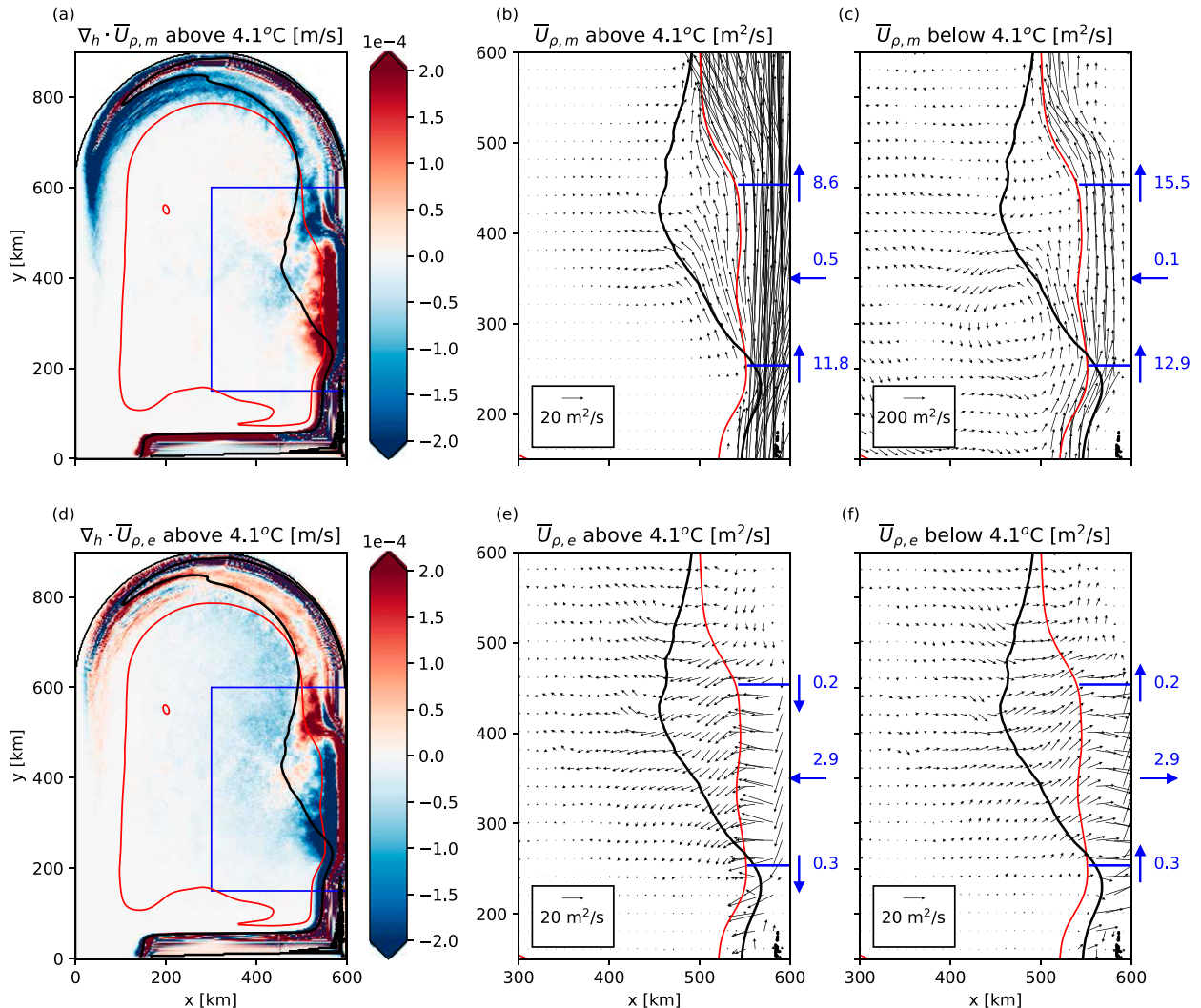
FIG. 5. Horizontal divergence of the isopycnal flow integrated over all layers above 4.1°C isotherm, decomposed into its (a) mean and (d) eddy component. Isopycnal flow above the 4.1°C isotherm, decomposed into its (b) mean and (e) eddy component. (c),(f) As in (b) and (e), but for the isopycnal flow below the 4.1°C isotherm. Note the different transport scale chosen in (c). The domain depicted in (b), (c), (e), and (f) is indicated by the blue rectangles in (a) and (d). The black contour indicates where the time mean depth of the 4.1°C isotherm intersects the time mean mixed layer depth; the red contour depicts the edge of the boundary current defined by the 24-Sv streamline of the barotropic streamfunction. Transports into the domain bounded by the red contour and the blue sections in (b), (c), (e), and (f) are given in blue (Sv).

current (Fig. 5a). Note that counteracting patterns can also be found in the northwest. This indicates that also within the remainder of the boundary current baroclinic instability is present, albeit weaker than at the narrowing because the horizontal density gradient is weaker.

In the northwest of the domain, the diapycnal downwelling shown in Fig. 3d is largely connected to the convergence of the mean flow (cf. Figs. 5a,d) owing to the permanent supply of warm water masses by the boundary current. In the interior, the convergence of the eddy flow dominates the local diapycnal water

mass transformation shown in Fig. 3d (cf. Figs. 5a,d). The eddy-induced water mass transformation in the interior (Fig. 5d) is mostly due to cooling within the anticyclonic warm-core eddies, which propagate from the narrowing into the interior and yield a supply of warm water. Once the water that is enclosed by the eddies gets colder than, for example, 4.1°C, there is a diapycnal flow from the layer warmer than 4.1°C into the layer colder than 4.1°C. How much heat the eddies lose and how cold they become depends on their route, propagation speed, and heat content. In general, one can observe that this water mass transformation in the

interior occurs farther westward for denser layers (cf. Figs. 3d–f), reflecting that the farther the eddies travel from east to west, the more heat they lose.

The decomposition of the isopycnal flow into its mean and eddy component (Figs. 5b,c,e,f) corroborates that the isopycnal exchange at the narrowing is eddy-driven (note the 10 times larger scaling of the vector field in Fig. 5c). While the mean flow (Figs. 5b,c) displays little exchange between the boundary current and the interior (0.5 Sv out of the upper layer and 0.1 Sv out of the lower layer), the eddy flow (Figs. 5e,f) displays a strong zonal component (2.9 Sv out of the upper layer and 2.9 Sv into the lower layer) that is typical for baroclinic instability: warm water masses are exported out of the upper layer of the boundary current and cold water masses are entrained into its lower layer (Khatiwala and Visbeck 2000). These results are in agreement with Cessi and Wolfe (2013) who found that the zonal residual flow within the lighter layers is directed out of the boundary current and for the denser layers, it is directed toward the boundary current. Since the eddies transfer dense water masses eastward along downward tilted isopycnals (cf. Fig. 3 and Fig. 5), the eastward eddy flow is also associated with downward motion which is most intense where a strong isopycnal tilt is accompanied by a strong eastward flow.

Unlike in the case of a restratifying convective patch, the water mass exchange along the boundary current does not lead to a collapse of the front since the front is permanently restored by the advection of warm waters from the south. Rather, the zonal water mass exchange changes the vertical distribution of the transport, resulting in barotropization as can be seen from the decrease of the upper layer mean flow along the boundary current (from 9.7 to 6.6 Sv) and an increase of the lower layer mean flow (from 12 to 15.3 Sv; see also section 4). Note that the eddies also change the density gradient between the boundary current and the interior so that the decreased thermal wind shear allows for weaker geostrophic velocities in the upper and stronger geostrophic velocities in the lower part of the boundary current.

d. Diapycnal and isopycnal changes in boundary current transport

In the remainder of this section, we quantify in more detail where the boundary current transport changes, and if this change results from diapycnal processes within the boundary current or an isopycnal exchange of waters with the interior. To this end, we separate the boundary current in small segments in alongshore direction. For each segment, the diapycnal boundary current transport change between two isopycnals ρ_1 and ρ_2 is calculated, based on Eqs. (1) and (3), as $\overline{w}_{\rho_1} - \overline{w}_{\rho_2}$.

The isopycnal transport change between the isopycnal layers ρ_1 and ρ_2 is calculated from the lateral transport $\overline{\mathbf{U}}_{\rho_1} - \overline{\mathbf{U}}_{\rho_2}$ across the boundary current perimeter (defined by the 24-Sv contour, see Fig. 2b). Finally, the total boundary current transport change (the sum of the other two) is derived from the alongstream transport divergence of $\overline{\mathbf{U}}_{\rho_1} - \overline{\mathbf{U}}_{\rho_2}$.

Figure 6a shows the diapycnal boundary current transport change as a function of distance along the perimeter and temperature (recall that in our setup this is equivalent to density). In agreement with the previous discussions, diapycnal water mass transformation from warmer into colder layers occurs all along the boundary current. Since the surface water masses of the boundary current cool along the perimeter, the water mass transformation takes place at lower temperatures in downstream direction. Notably, the coldest water masses (temperature below 4°C) are not affected by diapycnal mixing within the boundary current (Fig. 6a). Rather, these cold water masses are formed outside the stratified boundary current by deep convection in the interior (Figs. 3c,f), and are entrained into the boundary current along isopycnals as becomes clear from the isopycnal boundary current transport change (Fig. 6b). This isopycnal entrainment occurs primarily along the topographic narrowing, where the strong eddy activity leads to an enhanced outflow of boundary current water from warmer layers and to an enhanced inflow into colder layers (cf. Fig. 6b and Figs. 5e,f). We find similar but weaker isopycnal water mass exchange all along the boundary current (Fig. 6b), indicating that baroclinic instability is active all along the boundary current albeit weaker than at the narrowing.

The sum of isopycnal and diapycnal transport changes (Fig. 6c) depicts the barotropization of the boundary current transport (section 4). When integrated all along the boundary current (Fig. 6d), the boundary current transport of waters warmer than 4.1°C decreases and the transport of colder waters increases (green line). This transport increase of colder waters is due to two contributions of similar magnitude. First, the transport of waters between 4.1° and 3.9°C increases mostly due to diapycnal processes (blue line). It is slightly counteracted by a decrease in isopycnal transport for waters with temperatures down to 3.95°C (orange line). Second, the transport of waters between 3.9° and 3.7°C increases almost entirely due to the isopycnal inflow of waters into the boundary current (orange line).

Finally, the discrepancy between Eulerian downwelling and diapycnal downwelling becomes apparent when a two layer view in depth and isopycnal space is considered (Fig. 7). Along the narrowing, the transport in depth space in the upper 940 m is reduced by 5.5 Sv
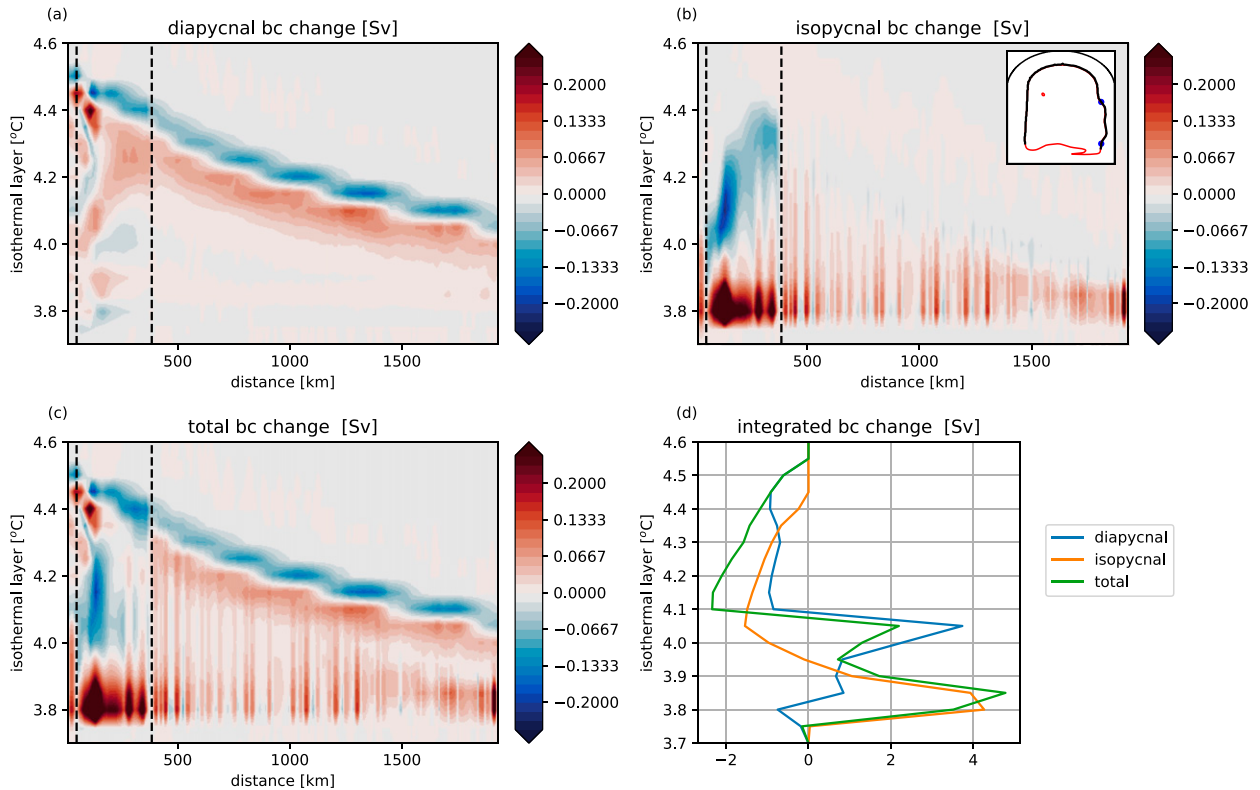
FIG. 6. Change in boundary current transport as a function of distance along the perimeter of the domain and for each isothermal layer, for (a) diapycnal flow, (b) isopycnal flow, and (c) their sum. (d) Net change in boundary current transport integrated along the basin perimeter, for (blue) the diapycnal flow, (orange) the isopycnal flow, and (green) their sum. The contour of the boundary current is indicated by 24-Sv contour line of the barotropic streamfunction in the inlay of (b); the black part of this contour corresponds to the part of the boundary current that is evaluated in this figure. The blue dots in the inlay of (b) and the vertical dashed lines in (a)–(c) indicate the region of the topographic narrowing.

(from 17.5 to 12.0 Sv) and it is increased by roughly the same amount in the lower 940 m upon passing the narrowing (Fig. 7, upper panels). There is only a rather small zonal flow of 0.4 Sv out of the boundary current above 940 m and a reverse zonal flow of 0.3 Sv below 940 m.

A considerably different picture emerges from the isopycnal view, quantified as the transport above and below the 4°C isotherm (Fig. 7, lower panels; the mean depth of the 4°C isotherm is closest to the depth level of 940 m). The transport in the upper isopycnal layer reduces by 6.1 Sv (from 16.8 to 10.7 Sv). This is not caused by a diapycnal flow from the upper into the lower layer; rather, there is a small diapycnal flux of 0.3 Sv from the lower into the upper layer as a consequence of vertical and biharmonic mixing (cf. Fig. 3e). Instead, the change of transport in the upper layer and lower layer is caused by a lateral isopycnal flow in and out of the boundary current of roughly 6.4 Sv.

The isopycnal viewpoint, which incorporates the effect of the eddies, clearly shows that the increase of

transport in the colder layer at the narrowing is due to the lateral inflow of dense water that was transformed in the interior or downstream of the boundary current, and that this increase is not due to a vertical diapycnal mass flux in the boundary current. Therefore, our diagnostics contradict the assumption inherent in the model of Straneo (2006) that assumes a direct diapycnal exchange of water from the upper lighter into the lower denser layer without any lateral exchange of water between the boundary current and the interior. Comparing the downwelling in density and depth space, we can conclude that both are fundamentally different with regard to where the downwelling happens but also how strong the downwelling is.

6. Pathways of convected water masses

In the previous section, we found that there are considerable differences regarding the Eulerian and isopycnal flow in a marginal sea that is subject to convection. In this section, we will further underline this
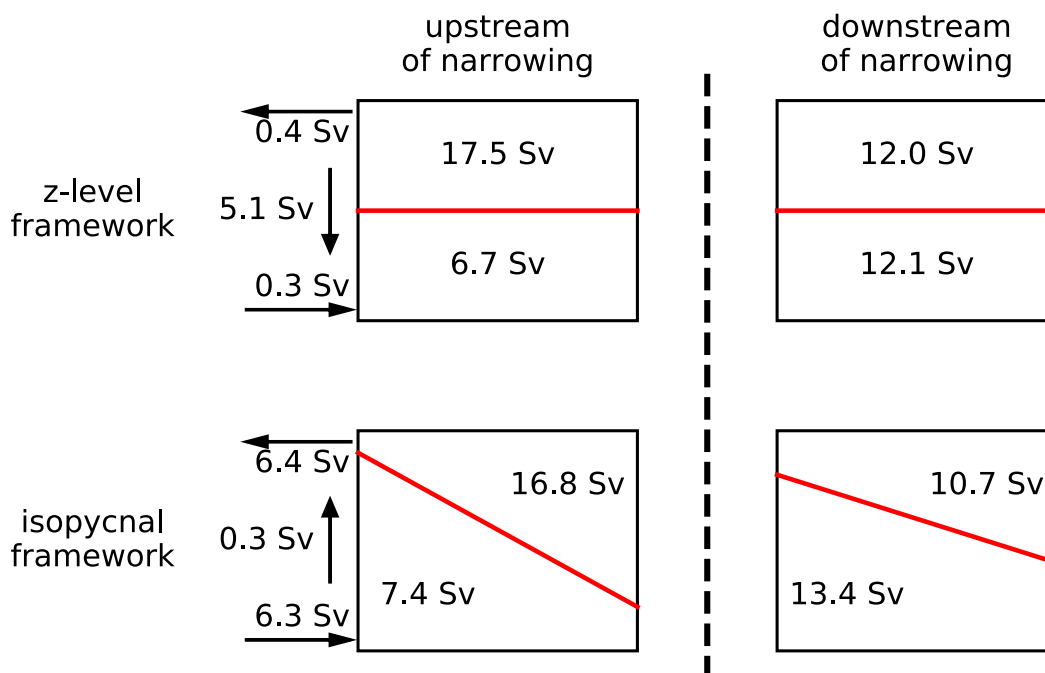
FIG. 7. Schematic of the Eulerian (top) time mean transports above and below 940 m and (bottom) time mean isopycnal transports above and below the 4°C isotherm. The situation (left) upstream and (right) downstream of the narrowing. The numbers within the rectangles indicate the meridional transport in the upper and lower parts of the boundary current. Horizontal arrows and numbers on the left indicate the zonal in- and outflow into the boundary current areal; the vertical arrow indicates the downward transport in depth space and isopycnal space, respectively (see text for a more detailed discussion).

by using passive tracers to study the pathways of water masses from their formation region (in the interior or the boundary current) toward the exit of the marginal sea via the boundary current.

To this end, we use three passive tracers that are restored to a value of one at the surface with a time scale of one day, and reset to zero in the restoring region. The tracer restoring is first introduced in year 10, after the flow has equilibrated, and maintained until year 12. To distinguish between water that is transformed in the interior and water that is transformed within the boundary current, we define three tracers: tracer 1 is only initialized over the boundary current, and tracers 2 and 3 only over the western and eastern half of the interior, respectively (red areas in insets of Figs. 8d–f). The water mass marked by tracer 1 can be exported out of the marginal sea directly by entering the restoring area; water masses marked by tracers 2 and 3 need to be laterally advected into the boundary current before they can leave the basin.

A snapshot of the three passive tracers (Fig. 8) already provides a good first impression of the pathways of the water masses. The concentration of tracer 1 (Figs. 8a,d), which is injected within 90-km distance of the boundary, displays the largest concentrations within the boundary current. Its concentration increases as the boundary current circulates around the basin. In the interior, the concentration of tracer 1 is much lower, but the snapshot shows that eddies are able to steer some tracer 1 into the interior as well (Fig. 8a). Notably, tracer 1 is hardly found below 1000-m depth (Fig. 8d). In particular, there is hardly any sign of tracer 1 in the east of the domain along the narrowing below the mixed layer. This emphasizes once more that there is no direct downward diapycnal transport of water along the narrowing, and thus no direct connection between the upper and the lower layer, at this region of the most intense downwelling in depth space (Fig. 1c).

In contrast, tracers 2 and 3 (Figs. 8b,c,e,f) do penetrate to depths below 1000 m. Particularly tracer 2, which is injected over the western half of the basin, reaches the densest isopycnal layers at the deep convection area in the southwest of the domain (Fig. 8e). From there, the horizontal snapshot suggests it is steered eastward mostly by the strongly sheared velocity field associated with the eddy field (Fig. 8b). It is remarkable that the concentration of tracer 2 even exceeds that of tracer 3 in the deep eastern part of the domain (Figs. 8e–f). The reason for this is that the stronger stratification in the eastern part of the domain caused by the eddy induced
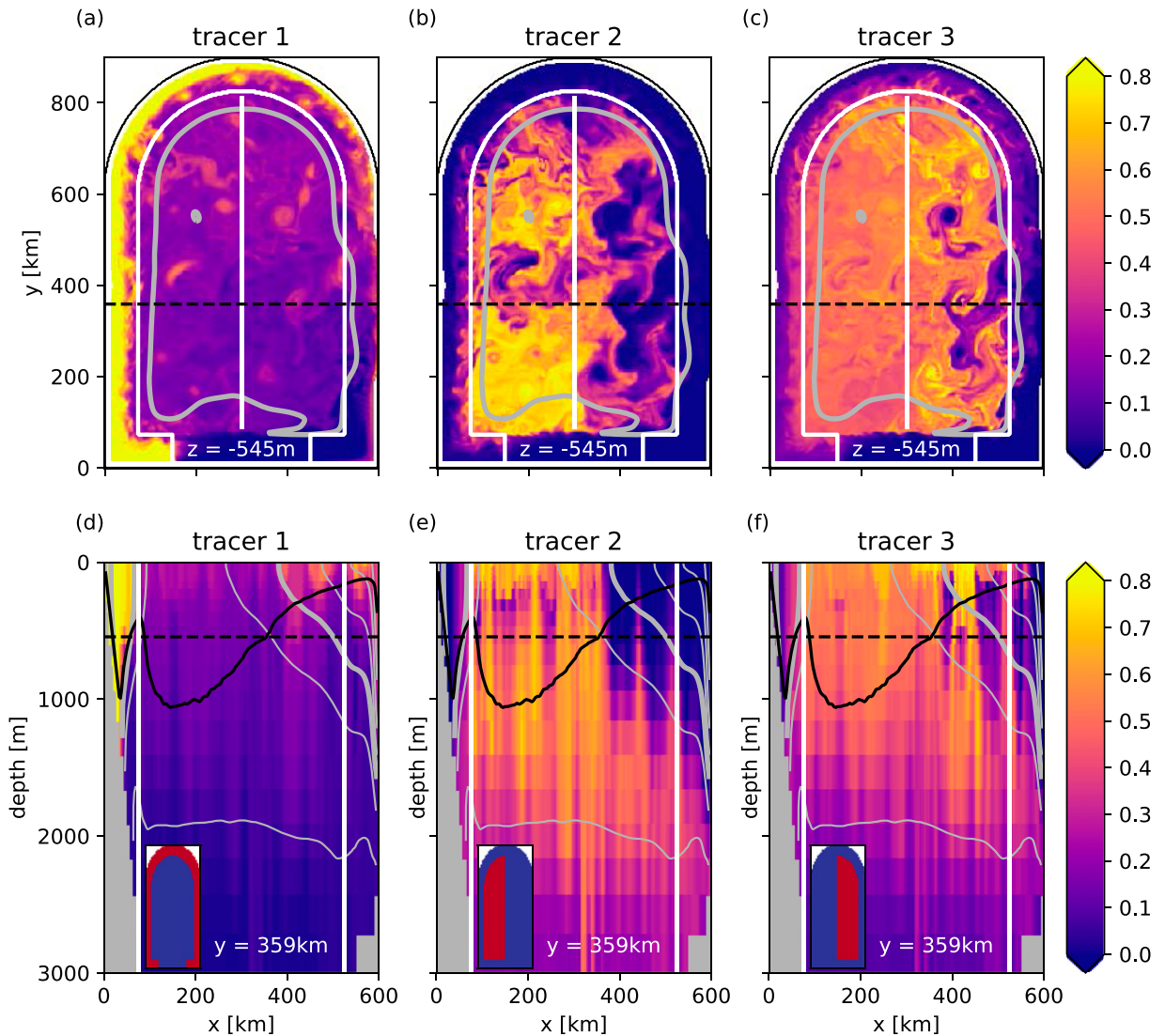
FIG. 8. Snapshots of the three different passive tracers (top) at 545-m depth and (bottom) for a zonal section at $y = 359$ km, 509 days after the release of the three tracers. These tracers mark water masses affected by diapycnal mixing (surface convection) in different regions (separated by the white lines): (a),(d) tracer 1–boundary current; (b),(e) tracer 2—western part of the interior and (c),(f) tracer 3—eastern part of the interior. The tracers are restored to one at the surface over the area depicted in the inlays of (d)–(f) and to zero in the restoring area over all depths. The gray line in (a)–(c) denotes the 24-Sv contour of the barotropic streamfunction. Gray lines in (d)–(f) denote time mean isotherms (contour interval is 0.1°C; thick gray line denotes the 4°C isotherm), and the solid black line denotes the mean mixed layer depth. Dashed horizontal lines in (a)–(c) denote the location of the transect in (d)–(f) and vice versa.

offshore advection of warm stratified waters which prevents tracer 3 from being directly mixed downward in the eastern part of the domain. Instead, tracer 3 first needs to be advected westward, convected downward in the less stratified western part of the interior, and advected back eastward. Obviously this route is not as efficient as that of tracer 2.

To underline the importance of the different tracer pathways for the tracer export of water masses transformed by convection, we integrate the tracer flux over time as it passes two dedicated sections through the boundary current (Fig. 9). The first section is chosen directly downstream of the narrowing, to analyze the tracer entrainment into the boundary current along the perimeter. The second section is chosen in the west, upstream of the restoring area, to highlight which water masses finally exit the marginal sea (see inserts in Figs. 9d–f).
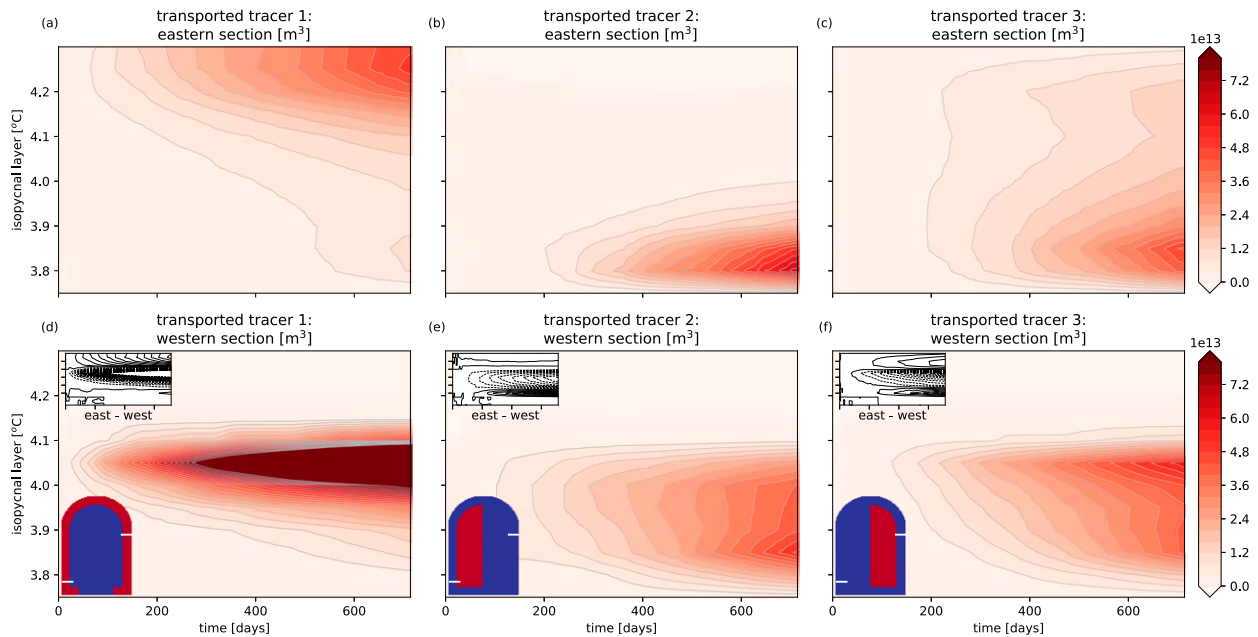
FIG. 9. Amount of tracer transported by the boundary current within different isopycnal layers, as a function of the tracer release time, for (a)–(c) a section in the east and (d)–(f) a section in the west, for tracers 1, 2, and 3 respectively. The amount of transported tracer M is defined as $M(\rho) = \int_0^t \int_{x_1}^{x_2} \int_{z(\rho)}^{z(\rho+\Delta\rho)} cv \, dx \, dz \, dt'$ with c denoting the tracer concentration, t is the time since the release of the tracer at year 10, x_1 and x_2 the start and end position of the section, and $\Delta\rho$ a density increment. Upper inlays in (d)–(f) indicate the transport differences between the eastern and the western section; the contour interval is $4 \times 10^{12}\,\mathrm{m}^3$, positive contours are solid, and negative contours are dashed. Lower inlays in (d)–(f) indicate the area where the tracers are restored and the locations of the two sections.

The transport of tracer 1 through both sections gradually increases from the beginning of the release (Figs. 9a,d). Notably, the transport at the western section is much stronger than in the east and occurs within colder isothermal layers. In contrast, the transport of tracers 2 and 3 at the eastern section mainly occurs within the coldest layers (Figs. 9b,c). At the western section, tracers 2 and 3 are also transported within intermediate layers (Figs. 9e,f) in addition to a transport within the coldest layers already seen at the eastern section. The timing of the tracer transport within the coldest isothermal layers indicates that tracers 2 and 3 first pass the eastern section before they arrive in the western section.

Based on the tracer export, we distinguish three different exit routes. The first exit route concerns lighter water masses (warmer than 4.0°C) that are formed directly in the upper layers of the boundary current by convection within the shallow mixed layer of the boundary current (tracer 1, Figs. 9a and 9d). Since the boundary current loses heat and its water masses are transformed into progressively colder water masses, these colder water masses are supplied with tracer and the tracer transport occurs within colder layers at the western section than at the eastern section (Figs. 9a,d).

The second exit route concerns water masses of intermediate densities (between 3.9° and 4.0°C; tracer 3 but to some degree tracer 2 as well, Figs. 9e and 9f). These water masses are formed in the interior but outside the deep convection areas in the southwest, where the stratification is weaker than in the boundary current but stronger than in the deep southwestern convection areas. After their formation, these water masses need to be advected into the boundary current to be able to exit the marginal sea. This entrainment most likely occurs all along the perimeter (see the gradual boundary current increase for layers of intermediate temperatures in Fig. 6b), resulting in a higher tracer transport at the western section than at the eastern section (cf. Figs. 9c,f).

The third exit route concerns the densest water masses (colder than 3.9°C) that are formed in the deep convection area, because everywhere else stratification prevents the coldest layers to be supplied by surface waters. In our setup, this exit route is mainly taken by tracer 2 (Fig. 9e) but to some extent also by tracer 3 (Fig. 9f). Eddies that approach the convective site from the east induce a strong velocity shear that stirs the tracer eastward along isopycnals out of the convection region. The more and more eddies approach from the topographic narrowing, the more and more the tracer is

consecutively mixed along isopycnals toward the narrowing. In this sense, eddies stir the dense water masses from their formation region toward the boundary current in the east. Since the isopycnals are strongly tilted downward in direction of the narrowing (see, e.g., Figs. 2c,d,f and 3a–c), the along-isopycnal eastward eddy transport also has a downward component as can be inferred from the tracer snapshots Figs. 8e and 8f that indicates a slantwise movement of the tracer. It can be as well inferred from the time series of the tracer transport Fig. 9. At the eastern section, the transport of tracer 2 and 3 is higher from day 200 onward for water masses colder than 3.9°C (cf. Figs. 9b,e, and Figs. 9c,f). This indicates that the bulk of tracer 2 and 3 arrives first at the narrowing where it is entrained into the boundary current, then circulates along the boundary before it arrives later at the western section. Regarding tracer 3, eddies need to steer this water mass first into areas with deep convection (Fig. 8c) from where these water masses then take the same route as those of tracer 2 [note the difference in timing: tracer 2 (Fig. 9b) appears to reach the eastern section sooner than tracer 3 (Fig. 9c)]. While the majority of the tracer is steered toward the narrowing in the east, there is also considerably weaker entrainment of tracer 2 (and 3) along the remaining perimeter.

Note that the relative efficiency of each pathway depends on multiple factors, for example, the strength of the surface heat loss, the stratification and strength of the boundary current, the location of the deep convection areas, and, especially, the location and strength of the eddy activity. In particular regarding the export of the densest water masses, the interplay between deep convection, isopycnal eddy stirring, and the boundary current transport is important: while deep convection forms the densest water masses, eddies are needed to steer these dense water masses into the boundary current. Finally, the latter is responsible for exporting these dense water masses out of the marginal sea.

7. Summary and conclusions

The main aim of this study is to investigate how and where water masses sink to large depths in a marginal sea that is subject to deep convection and displays enhanced eddy activity. To this end, we use an idealized model configuration of a typical marginal sea in the North Atlantic (e.g., the Labrador Sea or the Nordic Seas) that consists of a warm boundary current flowing along a topographic slope around a colder interior subject to strong surface cooling (Fig. 1). We particularly focus on discussing differences between the downwelling in depth space (i.e., the vertical mass flux through a certain depth level) and the downwelling in

density space (i.e., the transport from a lighter into a denser isopycnal layer). To this end, we find that the downwelling in depth space is fundamentally different from the downwelling in density space. While the former occurs predominantly within the deeper parts of the boundary current along the topographic narrowing, the latter occurs in the interior and in the upper part of the boundary current. In particular, there is no downwelling in density space along the topographic narrowing where the Eulerian downwelling peaks.

Furthermore, we identify two main mechanisms for the overturning in density space that are detailed in the schematic in Fig. 10: First, within the boundary current, the upper water masses are transformed into denser water masses as the boundary current cools along the perimeter due to surface heat loss and lateral eddy heat fluxes (Figs. 3 and 6a). The diapycnal processes at the surface allow the boundary current to cross isopycnals and therewith a flow from warmer into colder isopycnal layers. The export of these water masses is very efficient due to the high velocities within the boundary current, as illustrated by the high export rates of a tracer that is injected in the boundary current only (Figs. 6a,d). However, this export route only concerns the water mass transformation of lighter water masses since the boundary current stays relatively stratified along the basin perimeter (Fig. 6d). Notably, we find no major downward tracer transport along the topographic narrowing where the intense downward Eulerian flow is observed (Fig. 1c).

The second mechanism for overturning in density space involves water mass transformation by convection in the interior of the basin (Fig. 3) and a water mass exchange between boundary current and interior by eddies (Khatiwala and Visbeck 2000; Cessi and Wolfe 2013). Since the water in the interior is colder and far less stratified than the boundary current water, this process reflects the production of much denser water masses, in particular in the deep convection areas (Figs. 3f and 8e,f). However, these water masses need to be laterally advected into the boundary current to be exported out of the marginal sea. In our setup, this lateral advection is predominantly achieved by eddies originating from the topographic narrowing that steer these water masses toward the east into the boundary current (Figs. 6b and 5). Most of this transport occurs below the mixed layer where the eddies transport the tracer along isopycnals. Since the isopycnals are strongly tilted downward in the direction of the boundary current, an along-isopycnal flow obeys also a strong vertical component that is only present in the eddy component of the flow and not in the mean component. It is this combination of diapycnal downwelling and isopycnal
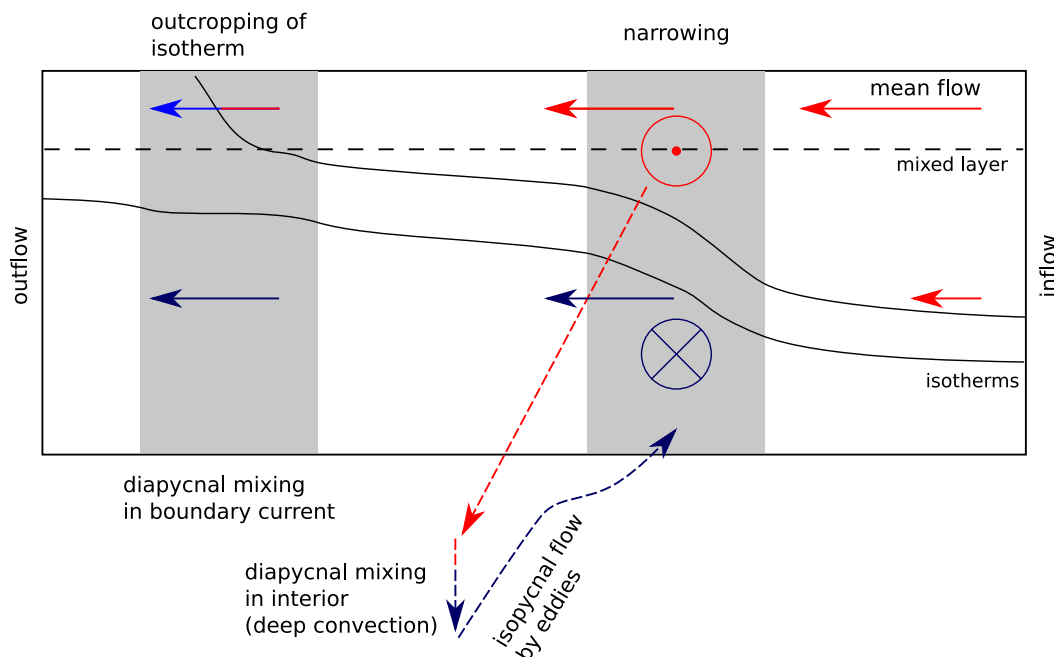
FIG. 10. Schematic of the residual overturning in a marginal sea with a strong eddy activity along the boundary current. It reflects: 1) Water mass transformation in the upper part of the boundary current where the warmer layers outcrop to the surface and the diapycnal processes at the surface allow the horizontal flow within the boundary current to cross isopycnals. 2) Water mass transformation in the interior by deep convection, where a lateral connection between the convection sites and the boundary currents by an isopycnal eddy flow along tilted isopycnals is essential to close the overturning loop.

downward eddy flow that manifests the downward limp of the residual circulation and we propose that this mechanism is key to the meridional overturning circulation of the North Atlantic.

The passive tracers that are injected over the convection region (tracer 2 and to some lesser degree tracer 3) reflect this pathway: the tracer is convected into dense isopycnal layers (Figs. 8e,f) and then laterally steered by eddies toward the narrowing and into the boundary current (Figs. 8b,c). Within the dense layers, the tracer therefore arrives first in the boundary current along the narrowing (Figs. 6b,c) before it appears further downstream at the western boundary (Figs. 6e,f).

The model simulation that we use is aimed to be an idealized representation of the circulation in a marginal sea characteristic for the North Atlantic. The idealizations that we applied certainly affect the outcomes quantitatively. For example, in reality, salinity plays a role for setting the stratification of the boundary current and for convection, if fresh stratified water from the boundary current is advected into the interior. In our study, we omit this aspect which might result in biases regarding the strength and location of convection. However, this does not affect the key features of the circulation that we aim to investigate: the presence of

deep convection and a strong eddy activity that allows for the exchange of water masses between a stratified boundary current and the convection areas.

Another simplification made in this study is that we do not consider any seasonality of the boundary current or the surface fluxes. Seasonality increases the complexity, since in a nonsteady case, the volume change of a water mass can be relevant as well [first term on l.h.s. of Eq. (2)] and diapycnal diffusive fluxes [r.h.s. of Eq. (2)] are not necessarily equivalent to diapycnal mass fluxes [second term on l.h.s. of Eq. (2)]. Therefore, diapycnal mass fluxes can have a different timing as or even occur at different locations than diffusive mass fluxes. Indeed, results from Xu et al. (2018) show that not all of the dense water masses that are formed in winter are exported at the same time but that some water masses are exported later in the year (their Fig. 20). Similarly, Pickart and Spall (2007) used an idealized model simulation of a marginal sea to show that the maximum heat flux into the marginal sea is slightly delayed from the period of surface cooling and lasting over the entire year. Spall (2015) showed that the response of the marginal sea depends on the strength of the eddy field and the frequency of the surface fluxes: while for high frequent forcing and a weak eddy activity the ocean

takes longer to adjust, there is an immediate response in case of low frequent forcing and a strong eddy field (our setup is an example of the latter). However, investigating the time dependency of the water mass export is beyond the scope of this study. Nevertheless, we find a qualitatively good agreement between the location where water masses are transformed in our setup and where this happens in the time dependent simulations of Xu et al. (2018). This leads us to assume, that including a seasonal cycle would not yield leading order effects on the qualitative mechanisms about how and where dense water masses are formed and exported.

The efficiency of the export route related to the eddy steering (route 2 in Fig. 10) strongly depends on the basin dimensions, the location of the deep convection area and the strength of the eddy shedding along the boundary current. In our setup, the eddy shedding peaks along the topographic narrowing, similar to the situation in the Labrador Sea or the Lofoten Sea. However, baroclinic instability can also generate eddies without such a topographic narrowing, for example, in the East Greenland Current (e.g., Fan et al. 2013). Such eddies might similarly contribute to an entrainment of dense water masses into the boundary current. The farther away the deep convection area is from the generation side of the eddies, and the less eddies are shed into the interior, the less of these water masses will be entrained into the boundary current. In this sense, the processes investigated here might be of relevance not only for the situation in the Labrador Sea or the Lofoten basin but also for other situations where buoyant boundary currents shed eddies and therewith increase the transformation of the buoyant water.

Note that the downwelling of roughly 6 Sv that we find in our setup is stronger compared to the overturning estimates of roughly 2 Sv measured in density space in the Labrador Sea (Pickart and Spall 2007; Lozier et al. 2019) and weaker than the estimate of 10 Sv obtained from the more complex global isopycnal model of Xu et al. (2018). Instead of tuning our simulation to specific observational estimates we designed our configuration such that it features strong convection and an intense eddy field. By doing this, we obtain a strong signal of the processes that we are investigating but also overestimate, for example, the eddy activity in the Labrador Sea.

Nevertheless, the qualitative aspects of the situation in, for example, the Labrador Sea are captured by our model as can be seen by comparing the diapycnal downwelling in our model with that of the more complex global isopycnal model of Xu et al. (2018). As discussed in section 5 diapycnal downwelling through an isopycnal in the boundary current only occurs where that isopycnal

crosses the base of the mixed layer (Fig. 3). An indication of that can be inferred from Fig. 12f of Xu et al. (2018) where diapycnal downwelling over the boundary current begins downstream of the West Greenland Current. In contrast, diapycnal downwelling in the interior is connected to the supply of buoyant water masses by eddies (Fig. 5). This is reflected in the simulation of Xu et al. (2018) where enhanced diapycnal downwelling in the interior of the Labrador Sea occurs in a region of high eddy kinetic energy (cf. their Fig. 12f and Fig. 17b). However, the approach of using an idealized configuration allows us to better observe the interplay between eddying circulation, convection, and downwelling compared to more complex models and observations where, for example, the bathymetry or temporally and spatially varying forcing complicate the interpretation.

Brandt et al. (2007) showed that most of the water masses that leave the Labrador Sea within two years were formed within the boundary current at its offshore flank at 55°W indicating a very efficient fast export route. However, there is also indication in Brandt et al. (2007) that even denser water masses were transformed in the interior of the Labrador Sea (their Fig. 11b). These water masses need to be laterally advected into the boundary current by eddies and thus take a longer export route: dense water that is entrained along the topographic narrowing along the West Greenland Coast indeed needs to circulate all along the basin perimeter before it can exit the marginal sea, so the different routes discussed in this study most likely represent different export time scales.

For the Southern Ocean, the difference between isopycnal and Eulerian circulation is known for quite some time and extensively discussed (e.g., Döös and Webb 1994; Olbers and Visbeck 2005). Our study emphasizes that also in the marginal seas of the North Atlantic a strong dissimilarity between isopycnal and Eulerian circulation (or equivalently between Eulerian and residual circulation) can be expected. This dissimilarity arises due to the bolus flow of the eddies (Khatiwala and Visbeck 2000) which needs to be added to the Eulerian mean flow to incorporate their effect on the circulation.

Despite the idealizations discussed above, our study bridges the gap between the Lagrangian picture obtained in Brandt et al. (2007) and the Eulerian picture obtained from idealized and realistic simulations (Spall 2004; Straneo 2006; Katsman et al. 2018; Waldman et al. 2018; Georgiou et al. 2019): the shedding of anticyclonic eddies toward the colder interior leads to a circulation that—when averaged over time—suggests a strong diapycnal downward flow. However, this downward flow does not reflect the actual pathways of water masses and therefore can be particularly misleading in the context

of the downwelling within a marginal sea that is subject to a strong eddy activity. Instead, water masses move along isopycnals when they are below the mixed layer and are better represented within the isopycnal framework. The latter indicates that diapycnal downwelling into the densest isopycnal layers does not occur within the boundary current but in the interior and eddies play a crucial role for exchanging these water masses between the deep convection areas and the boundary current.

REFERENCES

Abernathey, R., D. Ferreira, and A. Klocker, 2013: Diagnostics of isopycnal mixing in a circumpolar channel. *Ocean Modell.*, **72**, 1–16, https://doi.org/10.1016/j.ocemod.2013.07.004.

Adcroft, A., C. Hill, and J. Marshall, 1997: Representation of topography by shaved cells in a height coordinate ocean model. *Mon. Wea. Rev.*, **125**, 2293–2315, https://doi.org/10.1175/1520-0493(1997)125<2293:ROTBSC>2.0.CO;2.

Brandt, P., A. Funk, L. Czeschel, C. Eden, and C. W. Böning, 2007: Ventilation and transformation of Labrador Sea Water and its rapid export in the Deep Labrador Current. *J. Phys. Oceanogr.*, **37**, 946–961, https://doi.org/10.1175/JPO3044.1.

Cessi, P., and C. L. Wolfe, 2013: Adiabatic eastern boundary currents. *J. Phys. Oceanogr.*, **43**, 1127–1149, https://doi.org/10.1175/JPO-D-12-0211.1.

Dickson, R. R., J. Meincke, S.-A. Malmberg, and A. J. Lee, 1988: The great salinity anomaly in the northern North Atlantic 1968-1982. *Prog. Oceanogr.*, **20**, 103–151, https://doi.org/10.1016/0079-6611(88)90049-3.

Döös, K., and D. J. Webb, 1994: The Deacon cell and the other meridional cells of the Southern Ocean. *J. Phys. Oceanogr.*, **24**, 429–442, https://doi.org/10.1175/1520-0485(1994)024<0429:TDCATO>2.0.CO;2.

Fan, X., U. Send, P. Testor, J. Karstensen, and P. Lherminier, 2013: Observations of Irminger Sea anticyclonic eddies. *J. Phys. Oceanogr.*, **43**, 805–823, https://doi.org/10.1175/JPO-D-11-0155.1.

Gaspar, P., Y. Grégoris, and J.-M. Lefevre, 1990: A simple eddy kinetic energy model for simulations of the oceanic vertical mixing: Tests at station Papa and long-term upper ocean study site. *J. Geophys. Res.*, **95**, 16 179–16 193, https://doi.org/10.1029/JC095iC09p16179.

Gelderloos, R., F. Straneo, and C. A. Katsman, 2012: Mechanisms behind the temporary shutdown of deep convection in the Labrador Sea: Lessons from the Great Salinity Anomaly years 1968–71. *J. Climate*, **25**, 6743–6755, https://doi.org/10.1175/JCLI-D-11-00549.1.

Georgiou, S., C. G. van der Boog, N. Brüggemann, S. L. Ypma, J. D. Pietrzak, and C. A. Katsman, 2019: On the interplay between downwelling, deep convection and mesoscale eddies in the Labrador Sea. *Ocean Modell.*, **135**, 56–70, https://doi.org/10.1016/j.ocemod.2019.02.004.

Hall, M. M., D. J. Torres, and I. Yashayaev, 2013: Absolute velocity along the AR7W section in the Labrador Sea. *Deep-Sea Res. I*, **72**, 72–87, https://doi.org/10.1016/j.dsr.2012.11.005.

Holliday, N. P., S. Bacon, S. A. Cunningham, S. F. Gary, J. Karstensen, B. A. King, F. Li, and E. L. McDonagh, 2018: Subpolar North Atlantic overturning and gyre-scale circulation in the summers of 2014 and 2016. *J. Geophys. Res. Oceans*, **123**, 4538–4559, https://doi.org/10.1029/2018JC013841.

Jones, H., and J. Marshall, 1997: Restratification after deep convection. *J. Phys. Oceanogr.*, **27**, 2276–2287, https://doi.org/10.1175/1520-0485(1997)027<2276:RADC>2.0.CO;2.

Katsman, C. A., S. S. Drijfhout, H. A. Dijkstra, and M. A. Spall, 2018: Sinking of dense North Atlantic waters in a global ocean model: Location and controls. *J. Geophys. Res. Oceans*, **123**, 3563–3576, https://doi.org/10.1029/2017JC013329.

Khatiwala, S., and M. Visbeck, 2000: An estimate of the eddy-induced circulation in the Labrador Sea. *Geophys. Res. Lett.*, **27**, 2277–2280, https://doi.org/10.1029/1999GL011073.

Lozier, M. S., and Coauthors, 2019: A sea change in our view of overturning in the subpolar North Atlantic. *Science*, **363**, 516–521, https://doi.org/10.1126/science.aau6592.

Marotzke, J., and J. R. Scott, 1999: Convective mixing and the thermohaline circulation. *J. Phys. Oceanogr.*, **29**, 2962–2970, https://doi.org/10.1175/1520-0485(1999)029<2962:CMATTC>2.0.CO;2.

Marshall, J., A. Adcroft, C. Hill, L. Perelman, and C. Heisey, 1997: A finite-volume, incompressible Navier Stokes model for studies of the ocean on parallel computers. *J. Geophys. Res.*, **102**, 5753–5766, https://doi.org/10.1029/96JC02775.

McDougall, T. J., and P. C. McIntosh, 2001: The temporal-residual-mean velocity. Part II: Isopycnal interpretation and the tracer and momentum equations. *J. Phys. Oceanogr.*, **31**, 1222–1246, https://doi.org/10.1175/1520-0485(2001)031<1222:TTRMVP>2.0.CO;2.

Olbers, D., and M. Visbeck, 2005: A model of the zonally averaged stratification and overturning in the Southern Ocean. *J. Phys. Oceanogr.*, **35**, 1190–1205, https://doi.org/10.1175/JPO2750.1.

——, J. Willebrand, and C. Eden, 2012: *Ocean Dynamics*. Springer, 703 pp.

Pickart, R. S., and M. A. Spall, 2007: Impact of Labrador Sea convection on the North Atlantic meridional overturning circulation. *J. Phys. Oceanogr.*, **37**, 2207–2227, https://doi.org/10.1175/JPO3178.1.

Sayol, J.-M., H. Dijkstra, and C. Katsman, 2019: Seasonal and regional variations of sinking in the subpolar North Atlantic from a high-resolution ocean model. *Ocean Sci.*, **15**, 1033–1053, https://doi.org/10.5194/os-2019-27.

Send, U., and J. Marshall, 1995: Integral effects of deep convection. *J. Phys. Oceanogr.*, **25**, 855–872, https://doi.org/10.1175/1520-0485(1995)025<0855:IEODC>2.0.CO;2.

Spall, M. A., 2003: On the thermohaline circulation in flat bottom marginal seas. *J. Mar. Res.*, **61**, 1–25, https://doi.org/10.1357/002224003321586390.

——, 2004: Boundary currents and watermass transformation in marginal seas. *J. Phys. Oceanogr.*, **34**, 1197–1213, https://doi.org/10.1175/1520-0485(2004)034<1197:BCAWTI>2.0.CO;2.

——, 2010: Dynamics of downwelling in an eddy-resolving convective basin. *J. Phys. Oceanogr.*, **40**, 2341–2347, https://doi.org/10.1175/2010JPO4465.1.

——, 2015: Thermally forced transients in the thermohaline circulation. *J. Phys. Oceanogr.*, **45**, 2820–2835, https://doi.org/10.1175/JPO-D-15-0101.1.

——, and R. S. Pickart, 2001: Where does dense water sink? A subpolar gyre example. *J. Phys. Oceanogr.*, **31**, 810–826, https://doi.org/10.1175/1520-0485(2001)031<0810:WDDWSA>2.0.CO;2.

Straneo, F., 2006: On the connection between dense water formation, overturning, and poleward heat transport in a convective basin. *J. Phys. Oceanogr.*, **36**, 1822–1840, https://doi.org/10.1175/JPO2932.1.

Waldman, R., N. Brüggemann, A. Bosse, M. Spall, S. Somot, and F. Sevault, 2018: Overturning the Mediterranean thermohaline circulation. *Geophys. Res. Lett.*, **45**, 8407–8415, https://doi.org/10.1029/2018GL078502.

Walin, G., G. Broström, J. Nilsson, and O. Dahl, 2004: Baroclinic boundary currents with downstream decreasing buoyancy: A study of an idealized Nordic Seas system. *J. Mar. Res.*, **62**, 517–543, https://doi.org/10.1357/0022240041850048.

Xu, X., P. B. Rhines, and E. P. Chassignet, 2018: On mapping the diapycnal water mass transformation of the upper North Atlantic Ocean. *J. Phys. Oceanogr.*, **48**, 2233–2258, https://doi.org/10.1175/JPO-D-17-0223.1.

Young, W. R., 2012: An exact thickness-weighted average formulation of the Boussinesq equations. *J. Phys. Oceanogr.*, **42**, 692–707, https://doi.org/10.1175/JPO-D-11-0102.1.